Journal of Molecular Liquids 367 (2022) 120430

Contents lists available at ScienceDirect

Journal of Molecular Liquids

journal homepage: www.elsevier.com/locate/molliq

Vibrational dynamics of the OD stretch in an atomistic simulation of HDO in H_2O

Jesse Lentz, Stephen H. Garofalini *

Department of Materials Science and Engineering, Rutgers University, United States

ARTICLE INFO

Article history:
Received 9 May 2022
Revised 5 September 2022
Accepted 18 September 2022
Available online 23 September 2022

Keywords:
Molecular dynamics simulations
Frequency frequency correlation functions
HOD in H_2O

ABSTRACT

An all-atom molecular dynamics (MD) simulation of dilute HDO in H_2O was used to obtain vibrational frequency spectra from the classical MD trajectories and a wavelet-based method was developed to obtain the frequency-frequency correlation functions (FFCFs) of the OD stretch vibrations. Time constants were obtained on the order of 30 fs, 150–260 fs and 3.2–3.6 ps. An OD covalent bond length correlation function was calculated and a long-timescale decay constant of 1.73 ps was obtained, similar to experimental values that range from 1.45 ps to 1.8 ps. An O-O hydrogen bond length correlation function was calculated and found to exhibit an oscillation at 150 fs and a long-timescale decay time of 3.47 ps, both in good agreement with the FFCFs. Such results suggest that the spectral diffusion observed in FFCFs can be primarily attributed to fluctuations in O-O distances. An OD stretch energy correlation function was calculated, which consists of exponential decay with a time constant of 1.13 ps. The energy correlation function also exhibits two oscillations that are indicative of resonant energy transfer processes involving the OD stretch.

1. Introduction

The dynamically changing hydrogen bond structure and lifetimes affects many chemical and biological reactions. Understanding the variation of that h-bond structure, the interactions with the neighboring molecules, and the resultant spectral lifetimes adds important components to understanding the molecular behavior of water.

The hydroxyl stretch band of water reflects a wide range of local environments in the liquid. Low frequency hydroxyl stretches correspond to strong hydrogen bonds, whereas high frequency hydroxyl stretches correspond to weak or dangling bonds.[1–3] Spectral diffusion of the hydroxyl stretch therefore characterizes the timescale of fluctuations in the local structure, and can be quantitatively measured via a frequency-frequency correlation function (FFCF) [4]. Experimental FFCFs are obtained via time-resolved IR experiments. In order to probe the dynamics of a particular hydroxyl with minimal energetic coupling of the excitation, such experiments are commonly performed on dilute HDO in either H_2O [5–12] or D_2O [13–25].

The timescales of such experiments are limited by the vibrational lifetime of the hydroxyl stretch, which is obtained via pump-probe IR experiments. Steinel, et al. obtained a 1.45 ps lifetime for the OD stretch in H_2O, which is independent of excitation frequency. [10] Piletic, et al. reported a vibrational lifetime of 1.7 ps [11], and Kropman, et al. reported 1.8 ps [12]. The OH stretch of dilute HDO in D_2O has a comparatively short lifetime of less than 1 ps [14,16–19], making the latter system less suitable for the study of long-timescale spectral dynamics.

Vibrational echo correlation spectroscopy (VECS) experiments are believed to be the most accurate experimental probe of the spectral diffusion dynamics of the OD stretch in dilute HDO/H_2O [5–9]. The normalized FFCFs obtained from these experiments have been fitted to phenomenological tri-exponential models, the parameters of which have been compared to those obtained via MD simulations [5,6,8].

There are two classes of well-known methods for calculating hydroxyl stretch frequencies from classical MD simulations. The first is a hybrid classical-quantum method, in which the vibration of interest is modeled as a quantum mechanical oscillator coupled to a classical bath [6,13,26–29]. In the second method, DFT calculations are used to establish a statistical relation between hydroxyl stretch frequencies and their local electric fields [6,26,30–34] or electrostatic potentials [32]. In such a method, an ensemble of HDO configurations representing a variety of local structures is drawn from a classical MD simulation. For each configuration, DFT calculations are used to trace a potential energy versus

* Corresponding author.
E-mail address: shg@rutgers.edu (S.H. Garofalini).

https://doi.org/10.1016/j.molliq.2022.120430
0167-7322/

covalent bond length curve, from which a vibrational frequency is determined. From this ensemble of configurations, a linear relation is established between the electric field or potential on a hydrogen or deuterium atom and its instantaneous stretch frequency.

The ability of an MD model to reproduce experimental frequency spectra and spectral diffusion dynamics is a stringent test of its accuracy. The focus of the present work is therefore to test a classical, reactive, all-atom potential [35] which has been used previously to study bulk water [1], hydronium lifetimes[36], the water-silica interface [37–39], nano-confined water [40,41], dissolution of amorphous silica [42], and the water-vapor interface [37]. These processes and systems are highly dependent on the dynamics of water, and therefore the accuracy of the model's bulk water dynamics is of paramount importance. Because hydroxyl stretches are modeled classically, hydroxyl stretch frequencies and FFCFs can be directly calculated in this model from time-dependent covalent bond lengths.

2. Computational methods

A classical, reactive, all-atom water potential [35] was used, with an integration timestep of 0.1 fs. A system containing 4913 water molecules was initiated and run for 1 ps at 298 K and 1 atm in the constant number, pressure, and temperature (NPT) ensemble. At this stage, the atomic weights of nine randomly selected protons were set to 2, to produce nine HDO molecules. The deuterated system was then equilibrated for an additional 20 ps at the same temperature and pressure. The equilibration is performed using a canonical sampling through velocity rescaling (CSVR) thermostat [43]. The equilibrated system was continued for 100 ps at constant volume and energy (NVE), to produce a trajectory with one save per femtosecond (100,000 saves total).

For each OD group, a time-dependent frequency trajectory was calculated using a method based on continuous wavelet transforms. The continuous wavelet transform (CWT) of a time-domain function $r(t)$ is defined as follows [44,45]:

$$\Psi(\tau,s)=\frac{1}{\sqrt{s}}\int_{-\infty}^{+\infty} r(t)\psi^{*}\left(\frac{t-\tau}{s}\right)dt \tag{1}$$

In our case, $r(t)$ is the time-dependent covalent bond length of an OD group. $\psi(\xi)$ is a time-localized wavelet function, centered around $\xi=0$. The τ and s parameters translate and scale the wavelet, respectively, in the time domain. Both parameters have units of time. In practice, the integral of equation (1) can be taken between two points on opposite sides of the wavelet at which it has decayed to an infinitesimal magnitude; in the present work, it was evaluated around time τ from $t=\tau-500$ fs to $t=\tau+500$ fs. The simplified Morlet wavelet was used in this work, which is a complex exponential modulated by a Gaussian envelope [45], in which ω_o and ξ are unitless, is given by:

$$\psi(\xi)=\pi^{-\frac{1}{4}}\exp\left(i\omega_0\xi\right)\exp\left(-\frac{\xi^2}{2}\right) \tag{2}$$

The wavelet's oscillation frequency, expressed as a wavenumber k, is related to the scaling parameter, s, by the following relationship:

$$k=\frac{\omega_0}{2\pi cs} \tag{3}$$

where c is the speed of light, $2.998\times10^{10}\ \frac{\text{cm}}{\text{s}}$. ω_0 is a unitless parameter in the Morlet wavelet that controls the trade-off between temporal resolution (enhanced with low ω_0) and frequency resolution (enhanced with high ω_0). ω_0 is roughly equal to the number of sinusoid cycles inside the Gaussian envelope. In the present work, values of ω_0 ranging from 4 to 35 are used.

To calculate the OD's vibrational frequency at time τ, a 1 ps window centered around $t=\tau$ was taken from the $r(t)$ trajectory. $|\Psi(\tau,s)|^2$, as defined by Eqs. (1) and (2), was optimized along the s axis at a fixed value of τ. The first step of the optimization procedure was a grid search, using 101 evenly spaced s values, between values corresponding to $k=3400\ \text{cm}^{-1}$ and $k=1400\ \text{cm}^{-1}$, according to the relation shown in equation (3). $|\Psi(\tau,s)|^2$ was then maximized using the unconstrained Brent method [46], with a bracket defined by the maximal point found in the grid search and the two adjacent grid points. The SciPy [47] implementation of the Brent algorithm was used.

By this method, nine time-dependent OD vibrational frequency trajectories were obtained, from which frequency-frequency correlation functions (FFCFs) were calculated. Time points in the frequency trajectories, as well as in the resulting FFCFs, are spaced 5 fs apart. The FFCFs were calculated using the following equation:

$$C(t)=\frac{\left\langle\left(k_0-\bar{k}\right)\left(k_t-\bar{k}\right)\right\rangle}{\left\langle\left(k_0-\bar{k}\right)^2\right\rangle} \tag{4}$$

where k_0 is an OD's vibrational frequency calculated at time t_0, k_t is the same OD's frequency calculated at time t_0+t, and $\bar{k}$ is the average frequency over the whole ensemble. The correlation functions for OD covalent bond lengths and for hydrogen bond OO distances were calculated in an analogous manner to that shown in equation [4].

Each FFCF was fit to a biexponential ($n=2$) and a triexponential ($n=3$) model:

$$C(t)=\sum_{i=1}^{n} a_i\exp\left(-\frac{t}{\tau_i}\right) \tag{5}$$

where a_i are amplitudes and τ_i are the corresponding time constants. The fitting was performed using the Levenberg-Marquardt nonlinear least squares algorithm [48] as implemented by SciPy [47]. The initial parameter guesses for the biexponential model were $a_1=a_2=0.5$, $\tau_1=1.0$ ps, and $\tau_2=0.1$ ps; the initial guesses for the triexponential model were $a_1=a_2=a_3=0.33$, $\tau_1=1.0$ ps, $\tau_2=0.1$ ps, and $\tau_3=0.01$ ps.

Long-timescale decay constants were obtained from the OD covalent bond length correlation function, and from the O-O hydrogen bond length correlation function, by fitting the interval $0.5\ \text{ps}\le t\le 5$ ps to a single exponential term: $a\exp\left(-\frac{t}{\tau}\right)$. The Levenberg-Marquardt algorithm was used for these fits with initial guesses of $a=0.5$ and $\tau=1.0$ ps.

The OD stretch energy correlation function was calculated as well. The energy associated with an OD's stretch was expressed as $E=T+U$, where T and U are the kinetic and potential energy terms respectively. $T=\frac{1}{2}m_D\left[\left(\overrightarrow{v_D}-\overrightarrow{v_O}\right)\cdot\widehat{r_{OD}}\right]^2$, where m_D is the mass of deuterium, $\overrightarrow{v_D}$ and $\overrightarrow{v_O}$ are the velocities of the deuterium and oxygen atom respectively, and $\widehat{r_{OD}}$ is a unit vector pointing in the direction of the OD bond. $U=U_D-U_D^*$, where U_D is the potential energy of the system with the deuterium atom at its actual position, and U_D^* is the potential energy with the deuterium atom at the bottom of its potential well, with the positions of all other atoms held constant. The bottom of the potential well is assumed to be at position $\overrightarrow{r_O}+r_{OD}^*\widehat{r_{OD}}$, where $\overrightarrow{r_O}$ is the position of the oxygen and r_{OD}^* is the time-dependent equilibrium OD bond length. r_{OD}^* was optimized using the unconstrained Brent method [46] with a search bracket ranging from 0.88 Å to 1.08 Å. U_D and U_D^* were evaluated using only the potential's pair energy terms; the three-body energy was neglected. To validate this procedure, the mean and standard deviation (SD) of kinetic, potential, and total energy were

calculated over all saves and all OD bonds. In units of kT, $\langle T\rangle$ = 0.480 (SD: 0.503), $\langle U\rangle$ = 0.514 (SD: 0.485), and $\langle E\rangle$ = 0.995 (SD: 0.096). All three means are within 4% of the harmonic oscillator values as predicted by the equipartition theorem.

The OD stretch energy correlation function was modeled as the sum of an exponential decay term, $C_{exp}(t)$, and a non-exponential, oscillatory component, $C_{osc}(t)$. $C_{exp}(t)$ was obtained via a least squares fit between 0 and 1 ps, where it significantly exceeds the residual in magnitude. $C_{exp}(t)$ was subtracted from the original correlation function to obtain the residual, which was found to be dominated by a large oscillation at t = 2.7 ps and a smaller oscillation at t = 0.7 ps. $C_{osc}(t)$ was therefore modeled as the sum of two Ricker wavelets [45] and a constant. The constant is necessary because Ricker wavelets have a mean value of zero, and the mean value of the oscillatory residual is greater than zero. $C_{osc}(t)$ was fitted for $t \geq 0.1$ ps. The combined model is:

$$C(t) = C_{exp}(t) + C_{osc}(t)$$

$$C_{exp}(t) = a\exp\left(-\frac{t}{\tau_e}\right) \tag{6}$$

$$C_{osc}(t) = b_0 + \sum_{i=1}^{2} b_i\left(1 - T_i^2\right)\exp\left(-\frac{T_i^2}{2}\right)\left(T_i = \frac{t - \tau_{R,i}}{s_i}\right)$$

3. Results and discussion

Fig. 1a and 1b show the time-correlation function of OD covalent bond lengths. The vibrational stretch oscillations, with an average period of about 14 fs, can be seen in 1a. In 1b, the correlation function is smoothed using bins spaced at intervals of 50 fs, to remove the OD stretch oscillations and to highlight the picosecond-timescale decorrelation behavior. An exponential model was fit to the correlation function between t = 0.5 ps and t = 5.0 ps; the model is shown in Fig. 1b. It was fit using the original, unsmoothed correlation function.

The exponential fit produced a time constant of τ = 1.73 ps with an amplitude of 0.065. A single exponential term describes the long-timescale behavior of the OD correlation function reasonably well. Due to the anharmonicity of the OD potential, the mean covalent bond length increases both with increasing stretch amplitude and with decreasing h-bond distance [1]. Thus, fluctuations in both the OD's vibrational amplitude and in the O-O distance of its hydrogen bond should contribute to the OD correlation function's decay. As discussed later, the 1.73 ps time constant seems to be an average of both contributions. This time constant is similar to experimental OD vibrational lifetimes, which include 1.45 ps [10], 1.7 ps [11], and 1.8 ps [12,49].

Fig. 2 contains the OD stretch frequency spectrum obtained via Fourier cosine transforms of the deuterium velocity autocorrelation function (VACF) and of the OD bond length correlation function. In the figure, both spectra were smoothed by multiplying the correlation functions by Gaussian apodization functions of the form $\exp\left(-\frac{1}{2}\left(\frac{t}{\sigma}\right)^2\right)$. σ = 200 fs was selected to provide a reasonable level of smoothness. In the unsmoothed VACF-derived spectrum, the peak maximum occurs at 2501 cm^{-1} with a full-width at half maximum (FWHM) of 328 cm^{-1}. The apodization function red-shifts the peak maximum to 2473 cm^{-1} and broadens the FWHM to 342 cm^{-1}.

Schmidt, et al. calculated OD spectra of several water models including SPC/E, SPC/FQ, TIP4P, TIP4P/FQ, TIP5P/E, and Dang-Chang.[34] Our spectrum is broader and more red-shifted than those obtained using any of the aforementioned models. The broadest and most red-shifted frequency spectrum obtained by Schmidt et al. was that of the SPC/FQ model, which is centered at 2509 cm^{-1} (0.3% higher than ours) with a FWHM of 302 cm^{-1} (8% narrower than ours). The spectra obtained by Schmidt, et al. were calculated using instantaneous system geometries, and therefore are not motionally narrowed. Our spectrum was calculated using dynamical trajectories and therefore is motionally narrowed. Therefore, it is interesting that our spectrum is the broadest. This discrepancy may be partially due to the methodology of Schmidt et al., which is based on a linear model relating vibrational frequency to local electric field. The dispersion of vibrational frequencies about the regression line is ignored, which may narrow their spectra to some extent. However, the SPC/FQ IR and Raman peaks are respectively 11% broader[6,34] and 21% broader [34,50] than the corresponding experimental peaks, indicating that the underlying frequency distribution of SPC/FQ is most likely broader than can be experimentally justified.

Most of the spectra from Schmidt et al. exhibit shoulders on the blue side of their peaks, but our spectrum exhibits a far more significant sub-peak on the blue side. This sub-peak does not occur in the spectrum calculated from the covalent bond length correlation function, which is also shown in Fig. 2. Note that the latter is systematically red-shifted relative to the VACF-derived spectrum because the amplitude of OD vibrations inversely correlates with hydrogen bond strength, causing lower-frequency vibrations to be over-weighted in the covalent bond length correlation function.

Fig. 3 contains frequency-frequency correlation functions for values of the wavelet's window length parameter, ω_0, ranging from

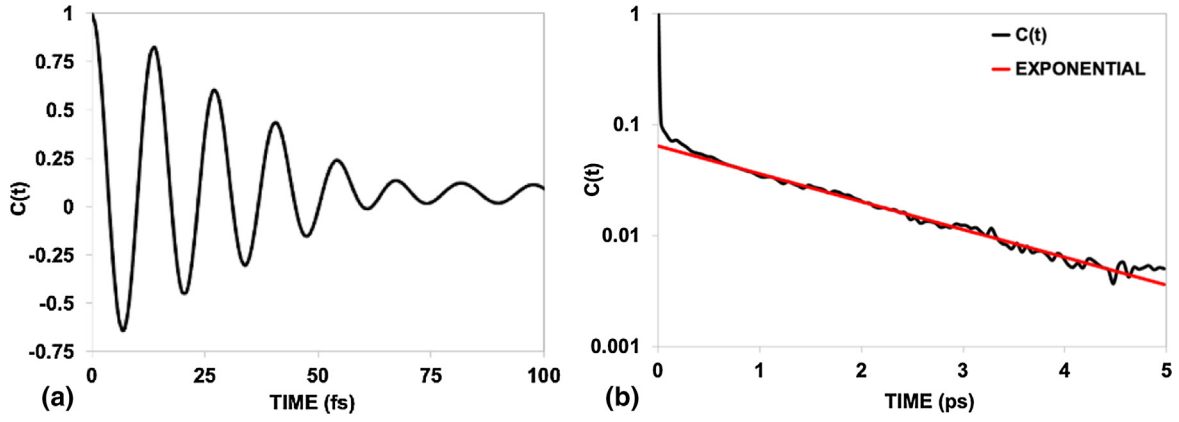

Fig. 1. The OD covalent bond length correlation function: (a) on a short timescale, showing femtosecond timescale oscillations due to OD stretch vibrations; (b) Smoothed version of the OD covalent bond length correlation function showing its picosecond-timescale decay together with an exponential model (τ = 1.73 ps).

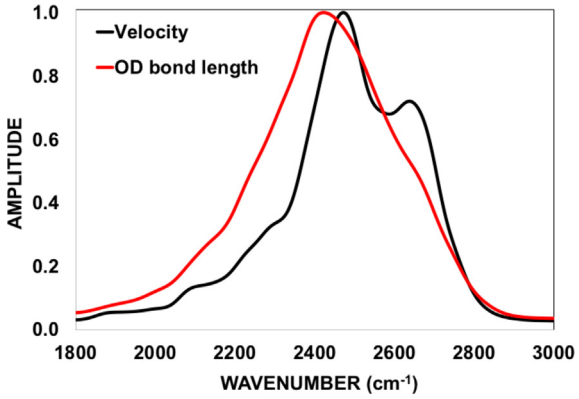

Fig. 2. OD stretch spectra obtained via Fourier cosine transforms of the deuterium velocity autocorrelation function and of the covalent bond length correlation function (shown in Fig. 1a). Note that the latter is systematically red-shifted due to the inverse correlation between vibrational frequency and stretch amplitude. Both spectra were smoothed using a Gaussian apodization function and normalized to have peak heights of 1.

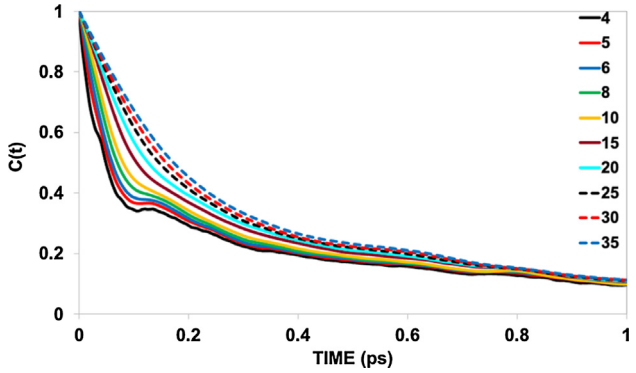

Fig. 3. Frequency-frequency correlation functions of the OD stretch vibrations, obtained using a series of wavelet lengths; ω_0 values range from 4 to 35.

4 to 35. The distribution of modal frequencies varies with ω_0; as ω_0 increases from 4 to 35, $\langle k \rangle$ increases from 2360 cm^{-1} to 2439 cm^{-1} while the standard deviation decreases due to motional narrowing. These data are reported in Table 1.

The FFCFs obtained using shorter wavelets ($\omega_0 < 10$) exhibit an oscillation at $t = 150$ fs. This oscillation is indicative of underdamped intermolecular OO vibrations, and corresponds to the oscillation observed in the OO distance correlation function shown later in Fig. 5. This oscillation occurs in the rigid, non-polarizable TIP4P and SPC/E models of water [30,34], but is absent in the polarizable SPC/FQ and TIP4P/FQ models [31,34]. For longer wavelets in the $\omega_0 > 10$ regime, the wavelets are sufficiently broad that these interatomic O-O vibrations are averaged over, and thus the FFCFs obtained using longer wavelets exhibit behavior which is closer to true exponential decay.

Table 1
Mean and standard deviation (SD) of the distributions of peak frequencies obtained using wavelets of various lengths.

ω_0	$\langle k \rangle$ (cm^{-1})	SD (cm^{-1})
4	2360.4	242.3
5	2389.3	237.2
6	2405.5	234.5
7	2415.2	232.7
8	2421.4	231.5
9	2425.8	230.0
10	2428.9	228.9
15	2436.0	225.0
20	2437.7	224.3
25	2437.9	225.0
30	2438.2	225.9
35	2438.6	226.3

Amplitudes and time constants were obtained using biexponential and triexponential fits to the FFCFs; these values are shown in Tables 2 and 3, respectively. The biexponential model underfits the data in the $\omega_0 < 10$ regime; this is apparent from visual inspection of the fits (see Fig. 4a), from the sum of the amplitudes (which differs significantly from unity for the low-ω_0 biexponential fits), and from the mean squared error (MSE) of the fits, which increase monotonically as ω_0 decreases in this regime. The $\omega_0 < 10$ regime corresponds to wavelets that are shorter than ~200 fs, while the shortest time constant observed in the triexponential fits lies in the 30 fs to 40 fs range; short wavelets require a triexponential model because they are sensitive to these fast frequency fluctuations, while longer wavelets average over these and require only a biexponential model. Fits for the $\omega_0 = 30$ FFCF are shown in Fig. 4b, with good agreement between the biexponential and triexponential models. In the analysis which follows, we consider the biexponential time constants valid for $\omega_0 \geq 20$. In the high-ω_0 regime, the triexponential models overfit the FFCFs because only two time constants are required. The triexponential models provide the lowest-MSE fit at $\omega_0 = 4$, with the MSE increasing monotonically as ω_0 increases from 4 to 35. The 30–40 fs range for the shortest time constant is comparable to the values of 44 fs and 53 fs found previously for TIP4P and SPC/E water respectively [30].

The long time constant of the FFCF has a plausible range from 3.2 ps to 3.6 ps (see Table 3). Experimental values from vibrational echo experiments include 1.4 ps [8], 1.5 ps [9], and 1.8 ps [5,6]. A spectral diffusion time of 2.0 ps [49] has been obtained from two-color pump-probe IR. MD simulations of TIP4P and SPC/E water have yielded time constants of 900 fs and 980 fs respectively [5,6,8], which are significantly faster than the experimental values. The polarizable SPC/FQ model has yielded a time constant of 1.45 ps [8,31], which is more consistent with experimental values. Our long time constant of >3 ps implies that our model has slower dynamics than polarizable rigid models, and significantly slower dynamics than non-polarizable rigid models. Our long time constants are also slower than corresponding experimental values by a factor of about 2, with the caveat that experimental measurement timescales are limited by the OD stretch lifetime of ~1.45 ps, so it is possible that experiments systematically underestimate the FFCF's long-timescale behavior.[6].

Our model's intermediate time constant has a plausible range from 150 fs to 260 fs. Vibrational echo experiments have yielded intermediate time constants of 300 fs [9] and 400 fs [5,6,8], while SPC/E and TIP4P have yielded 280 fs and 340 fs respectively [5,6,8]. SPC/FQ simulations have yielded intermediate time constants of 350 fs [8] and 352 fs [31]. Our intermediate time constant is therefore fast relative to other models and to experiments. Our short time constant, which is about 30 fs at low ω_0 values, is comparable to other models; SPC/E and TIP4P both predict 31 fs [5,6,8], while SPC/FQ predicts 48 fs [8,31].

As OD stretch frequencies have been shown to correlate significantly with OO distance [2,3], decorrelation of hydrogen bond distances is hypothesized to be a primary cause of spectral diffusion. Fig. 5a and 5b contain a correlation function of the oxygen-oxygen distance between a deuterium atom's covalently bonded oxygen, and the deuterium's next-nearest oxygen (i.e., its h-bond acceptor oxygen). Fig. 5a shows the effect of underdamped intermolecular vibrations with a period of 150 fs; this oscillation also appears in the FFCFs. Fig. 5b shows the decay due to longer-timescale processes, together with an exponential model of the long-timescale behavior. The exponential model was fit between $t = 0.5$ ps and

Table 2
Biexponential fit parameters of FFCFs obtained using wavelets of various lengths, and the mean squared error (MSE) of each fit.

ω_0	a_1	τ_1 (ps)	a_2	τ_2 (ps)	MSE (10^{-4})
4	0.18	2.63	0.62	0.10	3.13
5	0.19	2.62	0.67	0.10	2.94
6	0.19	2.67	0.70	0.10	2.77
7	0.19	2.71	0.72	0.11	2.65
8	0.19	2.74	0.73	0.11	2.56
9	0.19	2.80	0.74	0.12	2.43
10	0.19	2.84	0.75	0.12	2.33
15	0.19	2.99	0.78	0.14	2.07
20	0.19	3.08	0.79	0.15	1.94
25	0.19	3.12	0.81	0.17	1.83
30	0.19	3.14	0.82	0.18	1.97
35	0.19	3.15	0.83	0.19	2.14

Table 3
Triexponential fit parameters of FFCFs obtained using wavelets of various lengths, and the mean squared error (MSE) of each fit.

ω_0	a_1	τ_1 (ps)	a_2	τ_2 (ps)	a_3	τ_3 (ps)	MSE (10^{-4})
4	0.14	3.60	0.33	0.26	0.54	0.03	0.73
5	0.15	3.41	0.35	0.25	0.54	0.03	0.85
6	0.16	3.40	0.36	0.24	0.53	0.03	0.95
7	0.16	3.37	0.38	0.23	0.52	0.04	1.06
8	0.16	3.37	0.39	0.23	0.51	0.04	1.13
9	0.16	3.38	0.41	0.23	0.49	0.04	1.17
10	0.16	3.37	0.42	0.22	0.47	0.04	1.24
15	0.17	3.40	0.46	0.22	0.41	0.06	1.48
20	0.18	3.36	0.53	0.21	0.33	0.07	1.64
25	0.18	3.29	0.60	0.21	0.25	0.08	1.73
30	0.18	3.23	0.67	0.20	0.16	0.09	1.95
35	0.19	3.18	0.76	0.20	0.07	0.10	2.14

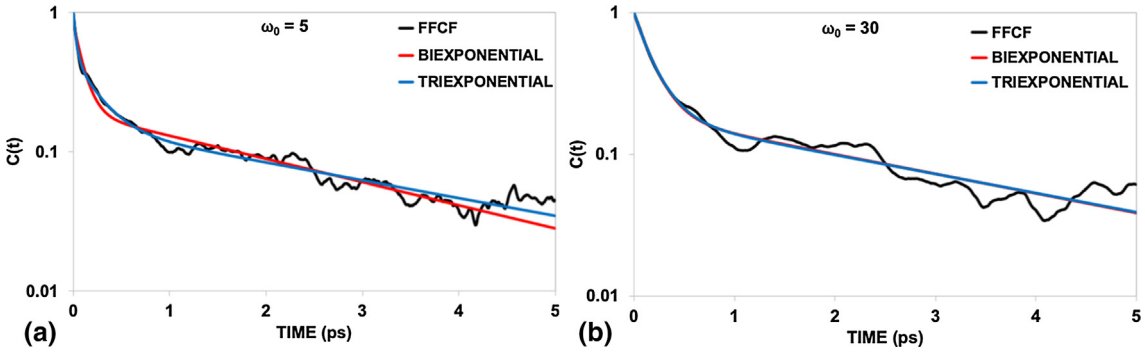

Fig. 4. Two FFCFs shown with their biexponential and triexponential fits, (a) $\omega_0 = 5$ and (b) $\omega_0 = 30$, to exemplify the short-wavelet and long-wavelet regimes, respectively.

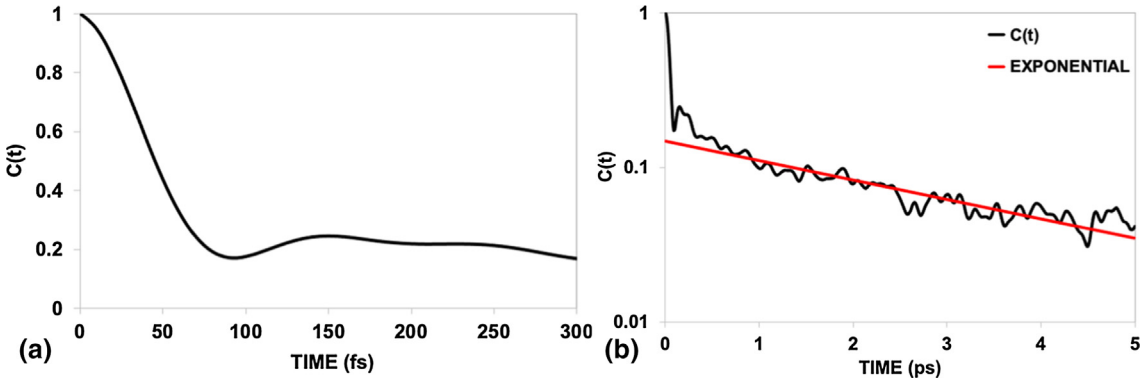

Fig. 5. Correlation function of oxygen-oxygen distances, where the two oxygen atoms are a deuterium atom's covalent oxygen and its next-nearest oxygen; (a) femtosecond-timescale intermolecular vibrations with a period of 150 fs, and (b) picosecond-timescale behavior shown with an exponential model ($\tau = 3.47$ ps).

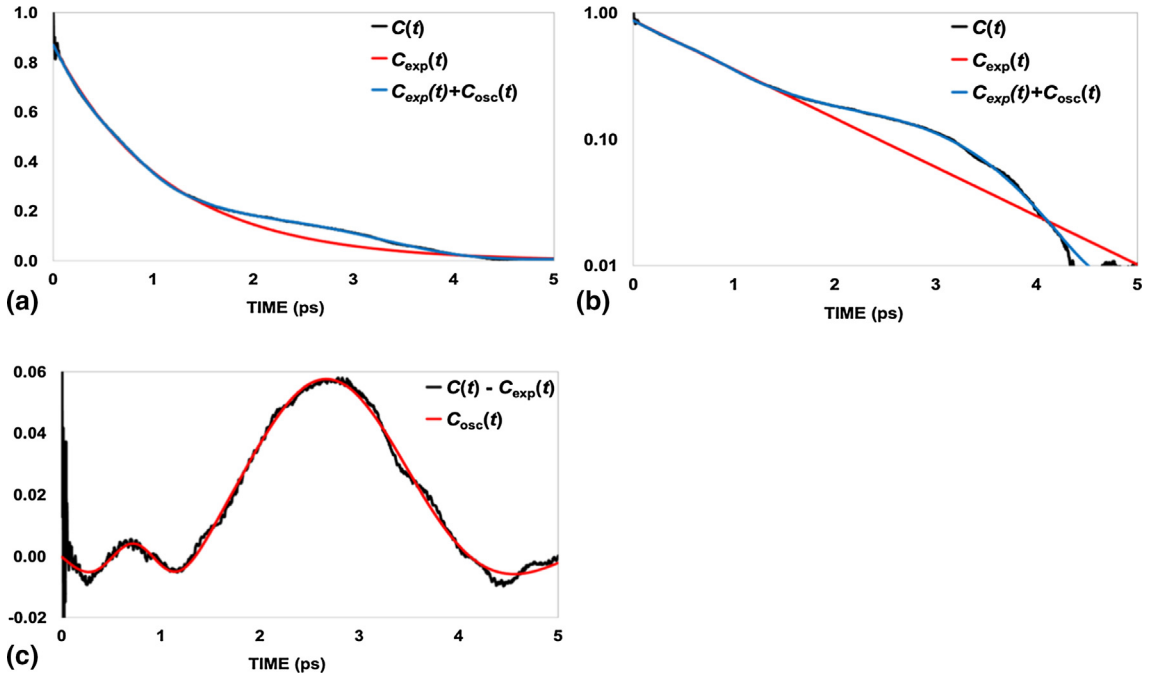

Fig. 6. OD stretch energy correlation function; (a) correlation function $C(t)$, exponential model $C_{exp}(t)$, and combined model $C_{exp}(t) + C_{osc}(t)$; (b) corresponding semi-log plot; (c) oscillatory residual of $C(t)$ together with oscillatory model $C_{osc}(t)$. Model components are listed in Table 4.

$t = 5.0$ ps. A time constant of 3.47 ps was obtained, with an amplitude of 0.15; this time constant is on the upper end of the range obtained from the FFCFs and is consistent with the hypothesis that spectral diffusion occurs primarily due to OO distance fluctuations.

The OD stretch energy correlation function and its model are shown in Fig. 6a-c. It is reasonably well-described by the model given in equation (6), consisting of a single exponential decay component and two oscillations, as shown in Fig. 6a and 6b. The parameters are shown in Table 4. A small oscillation occurs at 726 fs, and a significantly larger oscillation occurs at 2.7 ps, as shown in Fig. 6c. These oscillations can be interpreted as periods of resonant energy exchange processes involving the OD stretch mode. Vibrational relaxation of OD stretches in HDO have been experimentally shown to excite the HDO bending mode [51]. The 1.13 ps decay constant indicates that OD energy fluctuations occur somewhat faster than OD covalent bond length decorrelation, which has a time constant of 1.73 ps. This indicates that the OD covalent bond correlation time perhaps reflects an average between the energy fluctuation time and the OO fluctuation time, on both of which it depends. Compared to the energy correlation time, the OD bond length correlation time is more consistent with experimental OD vibrational lifetimes. [10–12,49].

Table 4
Parameters for the model of the OD stretch energy correlation function. See Eq. (6) for parameter definitions.

Parameter	Initial guess	Value
a	1.0	0.871
τ_e	1.0 ps	1.13 ps
b_0	0.0	0.0138
b_1	0.05	0.0439
$\tau_{R,1}$	2.7 ps	2.67 ps
s_1	1.0 ps	1.09 ps
b_2	0.01	0.00987
$\tau_{R,2}$	0.7 ps	0.726 ps
s_2	0.5 ps	0.313 ps

4. Conclusion

In this work, we performed a classical MD simulation of dilute HDO in H_2O using an all-atom potential. We developed a method for calculating time-dependent hydroxyl stretch frequencies from the classical MD trajectory by maximizing continuous wavelet transforms of time-dependent OD covalent bond lengths along the axis of the wavelet transform's scale parameter. These time-dependent frequency trajectories were used to calculate frequency-frequency correlation functions. These FFCF's were found to contain short (30–40 fs), intermediate (150–260 fs), and long (3.2–3.6 ps) time constants. The calculated OD stretch spectrum has a peak maximum at 2501 cm^{-1} and a FWHM of 328 cm^{-1}, which is lower-frequency and broader than frequency distributions obtained by Schmidt, et al. using a series of rigid water models [34]. From a time-correlation function of O-O hydrogen bond lengths, a time constant of 3.47 ps was obtained, which agrees well with the long time constants of the FFCFs, suggesting that the spectral diffusion observed in FFCFs can be primarily attributed to fluctuations in O-O distances. The OD covalent bond length correlation function has a time constant of 1.73 ps, which is similar to experimental OD vibrational lifetimes [10–12,49]. OD stretch energy correlation functions were also calculated; a time constant of 1.13 ps was obtained for OD stretch energy fluctuations, and two oscillations corresponding to resonant energy transfer processes were observed. O-O distance fluctuations in water are known to strongly affect energy barriers of proton transfer processes [36,52], while energy fluctuations enable protons to hop over the barrier; therefore, the present results have significant implications on the dynamics of autoionization and structural diffusion of H_3O^+ and OH^- ions in water. These results also demonstrate the ability of the employed classical water model to directly model the spectral dynamics of bulk water with reasonable accuracy, making it an effective model for the study of dynamical processes at water–mineral interfaces and in nano-confined water.

Declaration of Competing Interest

The authors declare that they have no known competing financial interests or personal relationships that could have appeared to influence the work reported in this paper.

Acknowledgements

The authors acknowledge support from the National Science Foundation (NSF) Environmental Chemical Science Program of the Division of Chemistry, grant number 1609044.

References

[1] J. Lentz, S.H. Garofalini, Structural aspects of the topological model of the hydrogen bond in water on auto-dissociation via proton transfer, Phys. Chem. Chem. Phys. 20 (24) (2018) 16414–16427.
[2] K. Møller, R. Rey, J. Hynes, Hydrogen bond dynamics in water and ultrafast infrared spectroscopy: A theoretical study, J. Phys. Chem. A 108 (7) (2004) 1275–1289.
[3] R. Rey, K.B. Møller, J.T. Hynes, Hydrogen bond dynamics in water and ultrafast infrared spectroscopy, J. Phys. Chem. A 106 (50) (2002) 11993–11996.
[4] J. Zheng, K. Kwak, M.D. Fayer, Ultrafast 2D IR vibrational echo spectroscopy, Acc. Chem. Res. 40 (1) (2007) 75–83.
[5] J.B. Asbury, T. Steinel, M.D. Fayer, Vibrational echo correlation spectroscopy probes of hydrogen bond dynamics in water and methanol, J. Lumin. 107 (1–4) (2004) 271–286.
[6] J.B. Asbury, T. Steinel, C. Stromberg, S.A. Corcelli, C.P. Lawrence, J.L. Skinner, et al., Water dynamics: vibrational echo correlation spectroscopy and comparison to molecular dynamics simulations, J. Phys. Chem. A 108 (7) (2004) 1107–1119.
[7] T. Steinel, J.B. Asbury, S.A. Corcelli, C.P. Lawrence, J.L. Skinner, M.D. Fayer, Water dynamics: dependence on local structure probed with vibrational echo correlation spectroscopy, Chem. Phys. Lett. 386 (4–6) (2004) 295–300.
[8] J.B. Asbury, T. Steinel, K. Kwak, S.A. Corcelli, C.P. Lawrence, J.L. Skinner, M.D. Fayer, Dynamics of water probed with vibrational echo correlation spectroscopy, J. Chem. Phys. 121 (24) (2004) 12431.
[9] S. Park, K. Kwak, M.D. Fayer, Ultrafast 2D-IR vibrational echo spectroscopy: a probe of molecular dynamics, Laser Phys. Lett. 4 (10) (2007) 704–718.
[10] T. Steinel, J.B. Asbury, J. Zheng, M.D. Fayer, Watching hydrogen bonds break: A transient absorption study of water, J. Phys. Chem. A 108 (50) (2004) 10957–10964.
[11] I.R. Piletic, D.E. Moilanen, D.B. Spry, N.E. Levinger, M.D. Fayer, Testing the core/shell model of nanoconfined water in reverse micelles using linear and nonlinear IR spectroscopy, J. Phys. Chem. A 110 (15) (2006) 4985–4999.
[12] M.F. Kropman, H.-K. Nienhuys, S. Woutersen, H.J. Bakker, Vibrational relaxation and hydrogen-bond dynamics of HDO:H_2O, J. Phys. Chem. A 105 (19) (2001) 4622–4626.
[13] C.J. Fecko, J.D. Eaves, J.J. Loparo, A. Tokmakoff, P.L. Geissler, Ultrafast hydrogen-bond dynamics in the infrared spectroscopy of water, Science 301 (5640) (2003) 1698–1702.
[14] R. Laenen, C. Rauscher, A. Laubereau, Dynamics of local substructures in water observed by ultrafast infrared hole burning, Phys. Rev. Lett. 80 (12) (1998) 2622–2625.
[15] R. Laenen, C. Rauscher, A. Laubereau, Local substructures of water studied by transient hole-burning spectroscopy in the infrared: Dynamics and temperature dependence, J. Phys. Chem. B 102 (1998) 9304–9311.
[16] S. Woutersen, U. Emmerichs, H.-K. Nienhuys, H. Bakker, Anomalous temperature dependence of vibrational lifetimes in water and ice, Phys. Rev. Lett. 81 (5) (1998) 1106–1109.
[17] G.M. Gale, G. Gallot, F. Hache, N. Lascoux, S. Bratos, J.-C. Leicknam, Femtosecond dynamics of hydrogen bonds in liquid water: A real time study, Phys. Rev. Lett. 82 (5) (1999) 1068–1071.
[18] G.M. Gale, G. Gallot, N. Lascoux, Frequency-dependent vibrational population relaxation time of the OH stretching mode in liquid water, Chem. Phys. Lett. 311 (3-4) (1999) 123–125.
[19] H.-K. Nienhuys, S. Woutersen, R.A. van Santen, H.J. Bakker, Mechanism for vibrational relaxation in water investigated by femtosecond infrared spectroscopy, J. Chem. Phys. 111 (4) (1999) 1494–1500.
[20] S. Woutersen, H.J. Bakker, Hydrogen bond in liquid water as a Brownian oscillator, Phys. Rev. Lett. 83 (10) (1999) 2077–2080.
[21] S. Bratos, G.M. Gale, G. Gallot, F. Hache, N. Lascoux, J.-C. Leicknam, Motion of hydrogen bonds in diluted HDO/D_2O solutions: Direct probing with 150 fs resolution, Phys. Rev. E 61 (2000) 5211–5217.
[22] G. Gallot, N. Lascoux, G.M. Gale, J.-C. Leicknam, S. Bratos, S. Pommeret, Non-monotonic decay of transient infrared absorption in dilute HDO/D_2O solutions, Chem. Phys. Lett. 341 (5-6) (2001) 535–539.
[23] J. Stenger, D. Madsen, P. Hamm, E.T.J. Nibbering, T. Elsaesser, Ultrafast vibrational dephasing of liquid water, Phys. Rev. Lett. 87 (2001) 027401.
[24] J. Stenger, D. Madsen, P. Hamm, E.T.J. Nibbering, T. Elsaesser, A photon echo peak shift study of liquid water, J. Phys. Chem. A 106 (10) (2002) 2341–2350.
[25] S. Yeremenko, M.S. Pshenichnikov, D.A. Wiersma, Hydrogen-bond dynamics in water explored by heterodyne-detected photon echo, Chem. Phys. Lett. 369 (1-2) (2003) 107–113.
[26] S. Li, J.R. Schmidt, S.A. Corcelli, C.P. Lawrence, J.L. Skinner, Approaches for the calculation of vibrational frequencies in liquids: comparison to benchmarks for azide/water clusters, J. Chem. Phys. 124 (20) (2006) 204110.
[27] C.P. Lawrence, J.L. Skinner, Vibrational spectroscopy of HOD in liquid D_2O. I. Vibrational energy relaxation, J. Chem. Phys. 117 (2002) 5827–5838.
[28] C.P. Lawrence, J.L. Skinner, Vibrational spectroscopy of HOD in liquid D_2O. II. Infrared line shapes and vibrational Stokes shift, J. Chem. Phys. 117 (19) (2002) 8847–8854.
[29] C.P. Lawrence, J.L. Skinner, Vibrational spectroscopy of HOD in liquid D_2O. III. Spectral diffusion, and hydrogen-bonding and rotational dynamics, J. Chem. Phys. 118 (1) (2003) 264–272.
[30] S.A. Corcelli, C.P. Lawrence, J.L. Skinner, Combined electronic structure/molecular dynamics approach for ultrafast infrared spectroscopy of dilute HOD in liquid H_2O and D_2O, J. Chem. Phys. 120 (17) (2004) 8107–8117.
[31] S.A. Corcelli, C.P. Lawrence, J.B. Asbury, T. Steinel, M.D. Fayer, J.L. Skinner, Spectral diffusion in a fluctuating charge model of water, J. Chem. Phys. 121 (18) (2004) 8897–8900.
[32] J.R. Schmidt, S.A. Corcelli, J.L. Skinner, Ultrafast vibrational spectroscopy of water and aqueous N-methylacetamide: Comparison of different electronic structure/molecular dynamics approaches, J. Chem. Phys. 121 (18) (2004) 8887–8896.
[33] S.A. Corcelli, J.L. Skinner, Infrared and Raman line shapes of dilute HOD in liquid H_2O and D_2O from 10 to 90 degrees C, J. Phys. Chem. A 109 (28) (2005) 6154–6165.
[34] J.R. Schmidt, S.T. Roberts, J.J. Loparo, A. Tokmakoff, M.D. Fayer, J.L. Skinner, Are water simulation models consistent with steady-state and ultrafast vibrational spectroscopy experiments?, Chem Phys. 341 (1) (2007) 143–157.
[35] T.S. Mahadevan, S.H. Garofalini, Dissociative water potential for molecular dynamics simulations, J. Phys. Chem. B 111 (30) (2007) 8919–8927.
[36] G.K. Lockwood, S.H. Garofalini, Lifetimes of excess protons in water using a dissociative water potential, J. Phys. Chem. B 117 (15) (2013) 4089–4097.
[37] J. Lentz, S.H. Garofalini, Formation and migration of H_3O^+ and OH^- ions at the water/silica and water/vapor interfaces under the influence of a static electric field: A molecular dynamics study, Phys. Chem. Chem. Phys. 22 (39) (2020) 22537–22548.
[38] G.K. Lockwood, S.H. Garofalini, Proton dynamics at the water-silica interface via dissociative molecular dynamics, J. Phys. Chem. C 118 (51) (2014) 29750–29759.
[39] J. Lentz, S.H. Garofalini, Role of the hydrogen bond lifetimes and rotations at the water/amorphous silica interface on proton transport, Phys. Chem. Chem. Phys. 21 (23) (2019) 12265–12278.
[40] S.H. Garofalini, T.S. Mahadevan, S. Xu, G.W. Scherer, Molecular mechanisms causing anomalously high thermal expansion of nanoconfined water, ChemPhysChem 9 (14) (2008) 1997–2001.
[41] S. Xu, G.W. Scherer, T.S. Mahadevan, S.H. Garofalini, Thermal expansion of confined water, Langmuir 25 (9) (2009) 5076–5083.
[42] M. Kagan, G.K. Lockwood, S.H. Garofalini, Reactive simulations of the activation barrier to dissolution of amorphous silica in water, Phys. Chem. Chem. Phys. 16 (20) (2014) 9294–9301.
[43] G. Bussi, D. Donadio, M. Parrinello, Canonical sampling through velocity rescaling, J. Chem. Phys. 126 (1) (2007) 014101.
[44] S.A. Mallat, wavelet tour of signal processing: The sparse way, 3rd ed:., Academic Press, Burlington MA, 2009.
[45] L. Debnath (Ed.), Wavelet Transforms and Their Applications, Birkhäuser Boston, Boston, MA, 2002.
[46] R.P. Brent, Chapter 4: An Algorithm with Guaranteed Convergence for Finding a Zero of a Function, Algorithms for Minimization without Derivatives, Prentice-Hall, Englewood Cliffs, NJ, 1973.
[47] P. Virtanen, R. Gommers, T.E. Oliphant, M. Haberland, T. Reddy, D. Cournapeau, et al., SciPy 1.0: Fundamental algorithms for scientific computing in Python, Nat. Methods 17 (3) (2020) 261–272.
[48] J.J. Moré, The Levenberg-Marquardt algorithm: Implementation and theory, in: G.A. Watson (Ed.), Numerical Analysis, Springer, Berlin, Heidelberg, 1978, pp. 105–116.
[49] R. Laenen, K. Simeonidis, A. Laubereau, Subpicosecond spectroscopy of liquid water in the infrared: Effect of deuteration on the structural and vibrational dynamics, J. Phys. Chem. B 106 (2) (2002) 408–417.
[50] J.D. Smith, C.D. Cappa, K.R. Wilson, R.C. Cohen, P.L. Geissler, R.J. Saykally, Unified description of temperature-dependent hydrogen-bond rearrangements in liquid water, Proc. Natl. Acad. Sci. 102 (40) (2005) 14171–14174.
[51] J.C. Deàk, S.T. Rhea, L.K. Iwaki, D.D. Dlott, Vibrational energy relaxation and spectral diffusion in water and deuterated water, J. Phys. Chem. A 104 (21) (2000) 4866–4875.
[52] D. Marx, M.E. Tuckerman, M. Parrinello, Solvated excess protons in water: quantum effects on the hydration structure, J Phys: Cond Matt. 12 (8A) (2000) A153–A159.